

## **Applications of SPOT-7 tri-stereo imagery in deriving the surface topography and mass changes of glaciers in Indian Himalaya**

**Vinay Kumar Gaddam<sup>a,b</sup>, Anil V Kulkarni<sup>c</sup>, Helgi Bjornsson<sup>d</sup>, Sriram Gullapalli<sup>e</sup>, Mallesh Ballina<sup>f</sup>**

<sup>a</sup>Department of Civil Engineering, DhaneKula Institute of Engineering and Technology, JNTU Kakinada, India

<sup>b</sup>National Center for Polar and Ocean Research, Ministry of Earth Sciences, Vasco -Da -Gama, Goa, India

<sup>c</sup>Divecha Center for Climate Change, Indian Institute of Science, Bangalore, India

<sup>d</sup>Department of Earth Sciences, University of Iceland, Iceland

<sup>e</sup>Geological Oceanography Division, National Institute of Oceanography, India

<sup>f</sup>Remote sensing department, Intergraph Hyderabad, India

Details of the corresponding author :Dr. G. Vinay Kumar,

Associate Professor, Department of Civil Engineering,

DhaneKula Institute of Engineering and Technology,

JNTU-Kakinada, India

Ph: 8975910989, email: gaddam\_vinay@ymail.com

### **Abstract:**

The present study describes the application of satellite images of SPOT 7, acquired on 10th October 2014 for producing the high spatial resolution digital elevation models of five glaciers in the Indian Himalaya. For data processing, we applied a Semi-Global Matching algorithm deployed in LPS-ERDAS. Ground control points were also used for validation, which were obtained during the autumn of 2014. Then, precise estimate is derived for the glacier area, the terminus elevation, the areas of supraglacial debris and the areas of proglacial lakes. Further, the ASTER (obtained in 2011) and SRTM V3 (of 2000) elevation models were used in conjunction with the generated SPOT-7 DEM to estimate the glaciers mass balance between 2000, 2011 and 2014. Mass balance was observed negative for all five glaciers, but the mass loss decreased from the mean of  $-0.99 \pm 0.27$  m.w.e.  $a^{-1}$  in 2000- 2011 to  $-0.61 \pm 0.31$  m.w.e.  $a^{-1}$  from 2011 to 2014.

**Keywords:** SPOT-7 DEM, SGM algorithm, Baspa basin, Western Himalaya.

## 1. Introduction:

High spatial resolution satellite images and their source Digital Elevation Models (DEM's) play a crucial role in mapping the earth surface features with a great accuracy, mainly the areal extents, mass movements, morphological changes of glaciers and perennial snow extents in the Himalaya (Maurer, 2016). Mapping of glacial area in the Himalaya at a high spatial resolution is essential because of the large discrepancies existing in the areal extents of glaciers made available by various glacier inventories (such as RGI, GSI, SOI, SAC-ISRO) for the Himalaya (Figures 1b,6a,b; RGI Consortium, 2017, SAC inventory, 2014, Sangewar and Shukla, 2009, SOI inventory, 1962). Due to the discrepancies in the areal extents, the assessment of availability of water budget becomes crucial for various socio-industrial activities to almost 1.4 billion people, located in the HKH region. Further, studies carried on mapping the glacier outlines in the Himalaya suggest frequent usage of Digital Elevation Model's at different scales (Jacobsen, 2004, Maurer, 2016). But, so far they are limited to the coarse resolution (Draugtet al. 2011). The DEM's can be created from various sources such as digitization using topographical maps (Burrough, 1986; Good child and Kemp 1990, Moore et al.1991), from field measurements using a total station or Global Positioning System (GPS) (Jacobsen, 2004), using Synthetic Aperture Radar (SAR) imagery, using LiDAR point cloud (Jacobsen, 2000) and by using satellite based optical stereo-photogrammetry (Jacobsen and Passini, 2003; Anant et al 2018). Among these, digitization of topographic data for producing the elevation model using topographic map or total station data is highly time consuming (Goodchild, 2008), whereas Synthetic Aperture Radar (SAR) datasets has poor object recognition and geometric location accuracy over the mountainous terrains, due to shadow and layover effects (Jacobsen, 2000). Moreover, the generation of Lidar point cloud is expensive. Hence, most of the applications rely on optical satellites based stereo products for extracting the DEM's (Li et al. 2004, Babu et al 2013, Rosenholm and Torlegard, 1988; Anant et al 2018). The advantages of stereo based elevation models are: 1) the wide coverage of the scene rather than restricted area, 2) the digital data that ease the automation process, and 3) regular temporal coverage with good spatial resolution. However, DEMs from stereo photogrammetry also suffers from shortcomings like computation time, accuracy and mainly, the presence of cloud cover or fog (Lee et al. 2000). During the past three to four decades, several space organizations like Indian Space Research Organization (ISRO), Airbus Defense (ADS), European Space Agency (ESA), National Aeronautics and Space Administration (NASA), Japan Aerospace Exploration Agency (JAXA) etc., have launched various optical satellites to provide the topographic information of earth's surface at different spatio-temporal and spectral resolutions (Jacobsen, 2004, Hayakawa et al. 2008). Among the datasets from these satellites, most

of the studies have used the elevation datasets from Advanced Space borne Thermal Emission and Reflection Radiometer (ASTER) and Cartosat because of their free availability and extensive geographical coverage (Ahmed et al 2007, San and Suzen, 2005, Toutin, 2008, Dandabathula, 2015, Babu et al. 2013; Narendra and Rao, 2006; Anant et al 2018). However, these DEMs are of coarse spatial resolution (~30m) and limited to study the changes occurred at sub-pixel level, especially for glacio-hydrological studies in the Himalaya, leading to uncertainty (Watson et al. 2019, Racovitenau et al. 2008).

Therefore, in order to produce High Resolution Satellite (1.5 meter) images (in mono, stereo and tri-stereo modes) with extensive geographical coverage world-wide, SPOT 6&7 satellite was invented by Airbus Defense and launched by ISRO using its PSLV in June 2014 (ADS, 2016). Standard data collection mode enables data acquisition in one pass i.e., North-South long strips of up to 600 km width. In addition, the high satellite agility allows very quick moves from one scene to another along an orbit. This provides capability to cover areas of more than 120 km x 120 km or 60 km x 180 km in a single pass. Also, corridor acquisition (non North-South oriented) allows rapid covering of certain areas in an effective way. Thanks to the on-board calibration technique of SPOT-6/7, since it provides the collection of pairs or triplets of images over areas of interest with the viewing angles between two consecutive images separated with only 15° or 20° and with a B/H ratio between 0.27 and 0.4 (Alganci et al. 2018). Thus the present study focuses on the applications of SPOT-7 tri-stereo pan merged multispectral (XMS) data for generation of a high spatial resolution elevation model (1.5m). Although, the work is concentrated on the generation of elevation models, few experimental results are also presented to illustrate the effectiveness of the high resolution images and generated elevation models in mapping glacio-morphological features such as areal extents, debris cover, snout positions and elevation changes of the glaciers located in Western Himalaya. Further, the generated DEM (2014) is used in conjunction with elevation models from Shuttle Radar Topography Mission (SRTM in 2000) and the ASTER (of 2011) to estimate the mass changes of these five glaciers between 2000 and 2014.

## **2. Study area**

Depending on the satellite data availability and previous estimates on mass balance, five glaciers were selected for the investigation (Figures 1a,b), namely Shaune garang, Jorya Garang, Naradu garang, Gor-garang and Gara glaciers, located in Baspa and Gara Kund basins of Western Himalaya. These glaciers are located in a geographical location, where the snow-accumulation is influenced by both the western disturbances and Indian Summer Monsoon (Dimri et al 2013). The altitude of these glaciers vary between 4500 and 5600 m.a.s.l, with an altitude difference of 1100

meters (Figure 4). Due to the high altitude, in-situ measurements are very sparse for estimation of the mass balance of these glaciers. Hence, most of the mass balance studies are carried out by remote sensing applications (Kulkarni et al. 2004, Gaddam et al. 2016, 2017a, Kaur et al. 2010). The total area of these glaciers is estimated to 28km<sup>2</sup>, and their Equilibrium line altitudes (ELAs) are estimated to 5100 m.a.s.l. Out of the five glaciers, four glaciers except Gor-Garang are north oriented glaciers. The south facing Gor-Garang has a heavy debris cover area and steep slopes.

### **3. Data:**

The tri-stereo images from SPOT 7 acquired on 10 October 2014 are selected ( 1b) for the generation of elevation models and mass balance evaluation. In addition, the ASTER DEM (obtained on 23<sup>rd</sup> October 2011) and SRTM V3 (acquired during 11-22 February 2000) are used in conjunction with SPOT-7 DEM to estimate the glaciers mass balance between 2000 and 2014.

### **4. Methodology:**

#### *4.1 Generation of elevation model:*

Many methods exists for image matching process and generation of digital elevation model using stereo images (Lucas and Kanade, 1981, Droj, 2008, Heid and Kaab et al, 2012). However, the least square image matching method was found to be successful for image matching process at a higher rate (Jacobsen, 2005), whilst, the radiometric differences of input images were not considered during this experiment. Further, Hirschmüller (in 2008) has invented a Semi-Global Matching algorithm for image matching process, which uses the pixel wise matching supported by a global smoothness function, optimized along multiple paths (Hirschmüller, 2011). It also has a regular algorithmic structure which uses simple operations and quite insensitive to the choice of parameters (Ernst and Hirschmüller, 2008; Hirschmüller and Scharstein 2009; Hirschmüller, 2011). Moreover, this method avoids the correlation problems caused by recording or illumination differences and facilitates matching at the boundaries of objects (Jacobsen, 2013). Hence, the Semi-Global Matching algorithm (fused in ERDAS Imagine Photogrammetry Suite) is preferred in the present study for DEM generation (Figure 2).

As a first step, the tri-stereo pair (Fore, Nadir and Aft) images were imported into the Leica Photogrammetric suite (LPS) as a new image block. During this process, the pyramids were computed for images to allow the faster display and easy handling. After importing, the interior and exterior orientations for the three images forming the block need to be estimated. This is because, the interior orientation defines the mathematical relationship between the camera, sensor, and the image model (pixel space); and the exterior orientation relates the sensor model via the image space

to the object model (ground space). Here, the interior and exterior orientation parameters required for the analysis are obtained from the Rational Polynomial Coefficients (RPC's), supplied in format of Extensible Markup Language (XML) along with the datasets. These RPCs define the initial functions for transforming the original sensor geometries into image geometries, and to orient the geometries of the block relatively to each other. However, the external orientation should be precise for pixel-based image matching and geo-referencing (PERKO et al., 2014). Hence, the initial RPC functions were refined with the help of ground control points (GCPs collected using field survey, ortho-photos) and tie points. The field GCPs (X, Y, Z coordinates) were manually collected through field survey in September 2014 by using Garmin GPSmap 76CSX, with a maximum RMSE of 8 meters (Gaddam et al 2016) and image coordinate points from orthorectified images at 1.5m spatial resolution, whereas Tie points through multi-image area-based correlation. Further, the three images were accurately tied and geo-referenced using least squares regression of the residuals of measured points, and then transformed the GCP coordinates.

Once the image triplet is accurately rectified, it is given to Semi-Global Matching algorithm as an input for generation of digital elevation model. During this process, the intensities of matched pixels are compared and the disparity (matching cost) is quantified, by resulting in a disparity image. In parallel, path wise optimization of a global cost function is conducted for each pixel. The disparity image pair is then compared pixel per pixel to detect inconsistencies and finally, delivers a 3D photogrammetric point cloud (\*.las), along with points at locations of consistent disparities.

#### 4.1.1 Uncertainty in DEM generation:

The accuracy of a DEM is mostly quantified by the Root Mean Square Error (Burrough, 1986, Wise, 2011, Heuvelink, 1998, eqn 1).

$$RMSE = \sqrt{\frac{1}{n} \sum_{i=1}^n (Z_{d,i} - Z_{r,i})^2} \quad - (1)$$

Where,  $Z_{d,i}$  is the 'i' th elevation value measured on DEM surface; and  $Z_{r,i}$  is the corresponding original elevation, and,, 'n' is the number of elevation points checked.

#### 4.2 Mapping of glaciers and its morphology:

The extraction of glacier margins is not possible by semi-automatic approaches like snow index (NDSI) in this study because of the absence of Shortwave Infrared wavelength region in the SPOT-7 dataset. Hence, the glacier margins are delineated manually using visual interpretation

techniques. Contrast [linear, photography adjustment] and brightness enhancement techniques are applied to the standard True Color Composite [Band combination: Green (0.53–0.590 $\mu$ m), Red (0.625–0.695 $\mu$ m) and NIR (0.76–0.890 $\mu$ m)] for the enhancement of the spatial and spectral quality of the image and for better interpretation. The snout positions could be identified accurately because of its high spatial resolution (1.5m) and with the help of geomorphic characteristics like (a) presence of ice wall (b) origin of river (c) red tone near the terminal moraines and (d) the presence of moraine-dammed lakes (Basnett et al. 2013). The ice divides (ice margins) in the upper ridges are interpreted by overlaying the pan merged multispectral image on the obtained DEM (with hill shade effect). After defining the snout positions and glacial extents, the glacier outlines are interpreted and then glacier's area is calculated. Similarly, the debris cover and lake extents present on the supra and peri-glacial zones are extracted manually. The uncertainties in mapping are estimated using Eqn. 2 (Gaddam et al. 2016).

$$\text{Mapping uncertainty (a)} = N * (A/2) \text{---(2)}$$

Where N is number of pixels along the glacier boundary

and A is the area of pixel

#### **4.3 Mass balance estimation:**

Mass balance is estimated using the geodetic approach for a period of 14 years, between 2000 and 2014. The elevation models from Shuttle Radar Topographic Mission (SRTM; obtained from <http://earthexplorer.usgs.gov/>) and Advanced Space borne Thermal Emission and Reflection Radiometer (AST14DMO, obtained from ([https://lpdaac.usgs.gov/dataset\\_discovery/ASTER/ASTER\\_products\\_table/ast14dmo\\_v003](https://lpdaac.usgs.gov/dataset_discovery/ASTER/ASTER_products_table/ast14dmo_v003))), having a spatial resolution of 30m are considered for mass balance estimation between 2000 and 2011, whereas the ASTER DEM (AST14DMO) and the elevation model generated in this study from SPOT-7 data (supplied by Airbus defense and Space, ottoburnn-Germany) is used to estimate the mass balance between 2011 and 2014. Further, to estimate the elevation changes uniformly, the spatial resolution of SPOT-7 DEM is resampled from 1.5 meter to 30 meters, which is equivalent to the spatial resolution of ASTER elevation image. However, in detail, these elevation models are developed using different techniques and offsets arise in both the horizontal and/or vertical axis while coregistration. For example, the elevation model of SRTM is generated using SAR interferometry by LPDAAC and the elevation models from ASTER and SPOT-7 are developed using stereo photogrammetry, by ASTER Science team and this study. Hence, the errors need to be removed/ minimized before the estimation of elevation changes (Berither and Toutin, 2008, Nuth and Kaab, 2011, Kaab et al.

2012). Therefore, the planimetric, across/along track and elevation dependent corrections are applied to remove the coregistration errors and then elevation changes are estimated. The process of estimation of elevation changes and mass balance is explained in sections 4.3.1 to 4.3.4.

#### 4.3.1 *Planimetric and across/along track corrections of DEM's:*

To perform the coregistration of the elevation models accurately and to remove the biases in horizontal (planimetric), vertical (elevation) and along/across the track, the Conventional Co-Registration (CCR) algorithm is applied. This CCR algorithm works on the characteristics relationship between elevation differences ( $dh$ ), terrain slope ( $\alpha$ ) and aspect ( $\psi$ ) (eqn 3; Figure 9). The cosine parameters ( $a, b$ , and  $c$ ) in eqn 1 are solved by using the Least Square Minimization algorithm. However, this analytical relationship is relied on terrain parameters and first solution is not the final result. Hence, several iterations of the process are required to minimize these cosine parameters, until the standard deviation is achieved to less than 2% or to a magnitude (of solve shift vector) which is less than 0.5 meters. Detailed explanation of the algorithm is given in Nuth and Kaab, 2011, Pieczonka et al. 2015.

$$dh / \tan(\alpha) = a * \cos(b - \psi) + c \quad \text{--- (3)}$$

Where ' $dh$ ' is individual elevation difference

' $a$ ' is magnitude of the horizontal shift

' $b$ ' is the direction of the shift vector

' $\alpha$ ' is the terrain slope and

' $\psi$ ' is the terrain aspect

For this study, SRTM and SPOT are considered as slave images and ASTER as the master image. As a preliminary step, the planimetric correction is applied on the stable terrain, by removing the non-stable terrain (glacial cover and river) from all the three elevation images. The glacier cover is removed using glacier mask (Gaddam et al. 2016) and river with 50 meter by river mask (from <http://gaia.geosci.unc.edu/rivers/>). Then the conventional algorithm is applied for planimetric adjustment (Figure 9; Nuth and Kaab, 2011, Bolch et al 2011). After applying this correction, the slave images (SRTM and SPOT) are shifted according to the positional vectors ( $\Delta x, \Delta y$ ). The bias rose along and across the satellite track was computed using the azimuth of ASTER and SPOT ground track and minimized by using a 4th order polynomial fit (Gaddam et al. 2017a, Gardelle et al. 2013). Further, the elevation dependent bias is reduced by removing the value of elevation

difference. Field control points obtained in the basin were also used during this process to minimize the error in elevation dependent bias

#### **4.3.2 Removal of outliers and estimation of elevation changes ( $dh$ ):**

The rectified slave images along with master (AST14DMO) image are considered further to estimate the glacier elevation changes ( $dh$ ), at an interval of 100m altitude bins. The elevation changes greater than +100m and lower than -100m are generally treated as outliers, since they represent the data gaps and DEM edges (Bolch et al. 2011). In addition to this, the pixels representing the absolute elevation difference more than  $3\sigma$  (three standard deviations) from the mean value are also discarded in each altitude bin. Then the mean elevation changes were analyzed (Figures 10a,b).

#### **4.3.3 Radar penetration:**

The elevation model of SRTM is acquired using C- band having a wavelength of  $\sim 5.6$  cm (NASA, 2000). The image acquisition using this wavelength region has a mean penetration of  $2.4 \pm 0.4$  meters over the snow surface of glaciers in the Lahaul-Spiti region (Gardelle et al. 2013, Gaddam et al. 2017a). Whereas, the radar penetration on debris covered ice/ablation zone generally remains negligible ( $\pm 0.4$ m; Rignot et al. 2001; Kaab et al. 2012, Wendt et al. 2017). Therefore, the elevation changes over the snow cover (accumulation) areas of the glaciers are corrected for radar penetration using the above said value by considering the mean equilibrium line altitude as 5100m (Table 2).

#### **4.3.4 Seasonality correction:**

The ASTER DEM is acquired in winter season (late October, 2011), whereas the SRTM is acquired in February, 2000. Since the acquisition period is in different time frames (October and February) of the year, the estimation of mass loss on an annual scale is difficult. Hence, seasonality correction is required. Therefore, the possible mass changes from October to February is derived from the mean winter mass balance of three glaciers (Gor-Garang, Shaune garang and Naradu) computed by temperature index model in the same basin for a period of 11 years between 2000 and 2011 (Gaddam et al. 2017a), which is estimated to  $+1.53 \text{ m.w.e.a}^{-1}$  (corresponding to  $+0.30 \text{ m.w.e.}$  per month). Also, it is observed that the estimated average winter mass balance is in good agreement with the modeled winter mean mass balance in Western Himalaya (Chhota Shigri glacier) during 2000-2009 ( $+1.17 \text{ m.w.e.a}^{-1}$ ) and 1969-2012 ( $+1.08 \pm 0.34 \text{ m.w.e.yr}^{-1}$ ) (Azam et al. 2014). However, the seasonality correction is not carried between 2011 and 2014, since the acquisition time frame is almost same (October). Further, the mean elevation changes among



various altitude bins are integrated throughout the glacier surface to estimate the volume change ( $m^3$ ), followed by mass balance estimation by approximating the density of ice as  $850 \pm 60 \text{ kg. m}^{-3}$  (Huss et al. 2013).

#### 4.3.5 Uncertainty estimation for mass balance and volume:

The uncertainties in volume ( $U_v$ ; eqn 4) and mass balance ( $U_m$ , eqn 5) were estimated by considering the error sources such as radar wave penetration ( $\Delta p$  in meters), relative vertical accuracy (Normalized Median Absolute Derivation – NMAD ( $\sigma \delta h$  in meters, which is resilient to outliers) and uncertainty in the ice density ( $\Delta \rho$  in  $\text{kg/m}^3$ ) (Bolch et al. 2011).

$$U_v = \sqrt{\Delta p^2 + \sigma \delta h^2} \text{-----} (4)$$

$$U_M = \sqrt{\Delta p^2 + \sigma \delta h^2 + \Delta \rho^2} \text{-----} (5)$$

#### 4.4. Debris cover mapping:

Mapping of debris cover is essential because, the presence of debris cover influences the glacier in two different ways. Thick debris cover retards the melting of underlying ice whereas the thin layer of debris accelerates the melting (Gaddam et al. 2016). Debris cover also alters the surface energy balance, as well as the sediment transportation capacity and may also lead to the glacier disintegration, if stagnant at terminus. Hence, mapping the debris cover is of utmost importance. However, mapping the supra-glacial debris cover extent by automated or semi-automatic technique is difficult. The studies carried out using these methods suggest that by applying appropriate threshold, the band ratio method can be used efficiently to delineate the supra-glacial debris cover. However, multispectral remote sensing data alone is not able to differentiate the supra-glacial debris from the neighboring periglacial debris (Shukla et.al. 2010). Hence, manual mapping of supraglacial debris is carried out in this study for the year 2014.

#### 4.5 Identification and mapping of lakes:

The lakes present on the supra-glacial zones of the glaciers influence the glaciers movement and lakes present in the pro-glacial zones (near terminus), which helps them to retreat faster, by supplying the heat flux from lake to the glacier (Basnett et al. 2013). Hence, mapping and monitoring the glacial lakes are required and carried out in this study by manual interpretation by using the 2014 spot imagery.

### 5. Results and Discussion:

#### 5.1 DEM generation:

In this study, the tri-stereo images of SPOT-7 are used for elevation model generation in the year 2014. The SPOT-7 is chosen for this study because of its unique characteristic “tri-stereo coverage”. The spot-7 sensor cover the same geographical location in three dimension from a single pass along one orbit, with viewing angles between two consecutive images as 15 or 20 degree and with the best B/H ratio of 0.27 and 0.4, where no other satellite provides the tri-stereo coverage with these unique capabilities. Here, the tri-stereo images of spot-7 are primarily matched to get a large number of automatically located conjugate points, by using Leica photogrammetric suite in Erdas. This process employs area-based matching in image pyramids and subsequently, local least squares matching by the SGM algorithm (Schrumiller, 2008). Once the images are resampled to epipolar geometries, the differences between RPC values and Y parallaxes were quantified according to the epi-polar images and minimized by performing the multiple block adjustments for the triplet. The initial RPC-based geolocation errors were reduced with the fine-tuning of RPCs using GCPs, as well as Tie Points (TP’s). The initial geolocation errors in x and y directions for measured GCPs (n=24) ranged from 4 to 13 m. Overall inaccuracies 5.4 (X-direction) and 11m (Y-direction) were observed consistent with the reported circular error of 8.5 m for spot imagery (Astrium- ADS,2012). When RPCs were refined with GCPs from field survey, geolocation accuracies for those points were improved and limited to  $\pm 8$  meters. The integration of TPs yielded another slight improvement of the GCP location accuracies. The solution with manually measured GCPs and numerous automatically derived TPs was used for the final triangulation of the block. The points were equally distributed across the glaciers to ensure a reliable rectification for all parts of the images. Then the image pairs are given as input to SGM for generation of a 3D point cloud, using a maximum disparity difference of 1. The results (\*.las files) are given in the Figure 3a and 3b.

The cloud consisted of 144 million points, with a point density of 5.22 per  $m^2$ , and was outputted in LAS format. In some areas, only few points could be correlated. Visual comparison of the satellite images and the point cloud showed that these data gaps coincide with image regions, where pixel intensities were significantly low due to shadow. Further, the outliers existing in this point cloud is removed by applying a local 3D filter, which identifies and removes the points having high positive and negative differences to the mean elevation of points in each 3D neighborhood. Through the filtering process, approximately 6% of points were identified as outliers and removed from the original output. The filtered point cloud was finally gridded to a 1.5 m DEM. It is observed that the mean elevation of the glaciers are varying between  $4450 \pm 6$  and  $5650 \pm 6$  meters above sea level (Figure 4; table 1). The variation of snout altitudes of these five glaciers since glaciation and at various time periods can be observed in the table 1.

### *5.2 Quantitative assessment of DEM:*

Quantitative assessment is carried for elevation points collected from SPOT-7 DEM and GCP's from field survey, conducted in September 2014, which suggested a good correlation (Figure 5) and also allowed for the calculation of mean error in elevation (Fisher and Tate, 2006).

### *5.3 Estimation of glacial area:*

The areal extents of GG, SG, JG, NG and GK glaciers are mapped manually and are estimated to  $4.05 \pm 0.34$ ,  $6.01 \pm 0.50$ ,  $10.37 \pm 0.86$ ,  $3.40 \pm 0.28$  and  $4.32 \pm 0.36$  km<sup>2</sup>. The terminus positions of the same are located at  $4703 \pm 6$  (GG),  $4505 \pm 6$  (SG),  $4447 \pm 6$  (JG),  $4513 \pm 6$  (NG),  $4712 \pm 6$  (GK) meters above sea level. The areal extents and terminus positions mapped by this study is slightly different than the previous reported literature (table 1; Figures 6a,b; Mir et al 2017, RGI 2015, Icimod, 2011). For example, the areal extents of Gor garang and Naradu garang glaciers mapped by Deota et al in 2011 are estimated to  $3.8 \pm 0.29$  km<sup>2</sup> and  $3.79 \pm 0.27$  km<sup>2</sup>. Similarly, the areal extents of Shaune and Jorya garang glaciers mapped by sangewar and shukla, 2009 are estimated to  $6.03 \pm 0.44$  and  $9.7 \pm 0.53$  km<sup>2</sup>. For Gara Kund, the area was mapped by Raina et al in 2000 and was estimated to  $4.28 \pm 0.22$  km<sup>2</sup>, respectively. The discrepancies rose in the areal extents can be attributed to different methodologies and differences in spatial resolution of the source images used in mapping methods. Moreover, the discrepancies can also be observed for the same glaciers by various international sources such as, GLIMS/RGI, ICIMOD etc. This is because, the mapping by GLIMS/RGI is carried by automated approach using coarse resolution Landsat datasets of the year 2000/2001 and ICIMOD by semi-automated approach. Mainly, the discrepancies can be observed in the ablation zone/debris covered ice regions of these glaciers and their tributaries. Overall, it is evident that the discrepancies is because of the a) difficulties in mapping the supra-glacial debris cover extent, b) spatial resolution of the source images used for mapping c) lack of field information and d) the disintegration of the glacier tongues, as the one observed in Shaune garang glacier. In the Shaune garang glacier catchment, the snow cover area on the left tributary of glacier could be mapped by only two studies (Figure 6a). Further, few tributaries of the same glacier is omitted as seen in the picture. Similarly, the debris covered area in the ablation area of Naradu glacier is omitted completely. Discrepancies can also be observed in the terminal position of Jorya garang and gor-garang glaciers (Figure 6b). The specific observations on the shift of terminus positions of the five glaciers are given in table1. Thus, mapping the areal extent and identification of terminal position of these glaciers are completely challenging using coarse resolution dataset because of the presence of heavy debris cover.

#### *5.4 Mapping Debris cover and lakes*

The areal extents of debris cover in this study is mapped for the year 2014 using manual interpretation and is estimated to 52% (GG), 38% (SG), 08% (JG), 31% (NG) and 14% (GK), respectively (Figure 7). Among these five glaciers, Gor Garang has higher percentage of supraglacial debris extent. Whereas, the supraglacial lakes on Naradu and Gor-Garang glaciers, and Proglacial Lake, which is associated with Shaune Garang terminus are mapped using the same time period imagery. The areal extents of supraglacial lakes on Gor-garang and Naradu glaciers are estimated to  $29000 \pm 400 \text{ m}^2$  (minimum glacial lake area in the basin) whereas the lakes in proglacial area of Shaune garang glacier is estimated to  $67000 \pm 1690 \text{ m}^2$  (maximum glacial lake area in the basin), respectively (Figure 8). Moreover, these lakes may expand its area in near future due to ongoing changes in climate (Gaddam et al. 2017a) and helps the glaciers to retreat faster, as the ones observed on the Changme Khangpu glacier, Eastern Himalaya (Basnett et al. 2013).

#### *5.5 Estimation of elevation changes and mass loss:*

The elevation models of SRTM, ASTER and SPOT-7 are used to estimate the elevation changes and mass loss of the selected glaciers, in two time intervals between 2000 and 2011 (SRTM-ASTER) and from 2011 to 2014 (ASTER-SPOT7). During the coregistration process, the slave images (SRTM and spot-7 dem's) exhibited distortions compared to the master (ASTER) image. The SRTM exhibited higher distortions (X: 48.8", Y: 6.6" and Z: 8.8m), and the spot exhibited minimal distortions (X: 18.6", Y: 2.8" and Z: 6.9m). The Figure 9 represents the modeling registration induced error of ASTER DEM with SRTM DEM (2000-2011), and ASTER DEM with SPOT-7 DEM (2011-2014).

The elevation changes estimated before co-registration for the two time intervals is observed higher. A change of -180m to +180m is observed for a period of 11 years, between 2000-2011 and from -79m to +63 meter for a period of 3 years, between 2011 and 2014. However, these elevation changes suggest the presence of artefacts and outliers. Hence, they are removed by the co-registration process using conventional correlation algorithm. Thus, the outliers are removed and then the elevation differences (dh) are estimated. The elevation differences after the coregistration process is observed between  $\pm 49\text{m}$ , between 2000 and 2011, whereas between  $\pm 10$  meters, between 2011 and 2014 (Figures 10a and 10b).

The elevation changes suggest thinning in the ablation areas and thickening in the accumulation areas (Figures 10a, 10b) for both the observation periods. However, thinning can also be observed in accumulation zones, having steep slope area. This may be because of the snowpack erosion to lower altitudes, due to gravitational pull. The accumulation is observed for all the five

glaciers, where little/negligible accumulation is observed for gor-garang glacier. For the same glacier, thickening is observed on the surface area between 2000 and 2011, because of deposition of debris cover from surrounding rock wall and expansion of lake area in the upper accumulation zone (Figures 8, 10a). Overall, the maximum surface elevation changes are observed for Gor-garang glacier. From the observations of the elevation changes and lakes formation on this glacier, it is strongly evident that this glacier may react faster to ongoing climate change and may lead to the supraglacial lakes formation. Further, the elevation changes are integrated throughout the surface to calculate the mean mass balance, by the assumption of ice density as  $850 \pm 60 \text{ kg/m}^3$  (Gaddam et al. 2017a).

Mass balance is observed negative for all five glaciers, during the study period (table 2). During 2000 and 2011, the mean annual mass balance for the glaciers is observed to be varying between  $-0.83$  to almost  $-1.19 \text{ m.w.e.a}^{-1}$ , with an estimated uncertainty of  $\sim 0.3 \text{ m.w.e}$ . Whereas, during 2011 to 2014, it is observed varying from  $-0.40 \pm 0.24$  to  $-0.9 \pm 0.25 \text{ m.w.e}$ . Comparative analysis is carried for estimated mass balance measurements of five glaciers in this study with measurements of same glaciers from existing literature, to find the agreement between the values and to understand the climatic impact on glaciers melt (table 2). It is observed that the estimated mass balance values are in good agreement with the published estimates of the glaciers in the same basin ( $r > 0.8$ ; Prasad et al 2019; Kumar et al 2018; Gaddam et al 2017a; Pratap et al 2016). Also, it is evident that the mass balance during past decades (1970's to 1990's) were lower than the present mass balance values, which suggests a climatic impact on the glaciers in this valley in the recent decades (Gaddam et al 2016). However, the estimates of mean mass loss ( $-0.61 \pm 0.31 \text{ m.w.e.a}^{-1}$ ) in the recent period 2011-2014 suggests that the mass loss is decreased, when compared with mass balance values of the same glaciers between 2000 and 2011 ( $-0.99 \pm 0.27 \text{ m.w.e.a}^{-1}$ ).

## **6. Conclusion:**

This study explores the application of SPOT-7 satellite stereo pairs for studying the topographical characteristics and mass balance of Himalayan glaciers. The 3D terrain information is generated by the application of Semi-Global matching algorithm. Despite the complex topography of the selected high-alpine site, the produced point cloud and the derived 1.5 m DEM included accurate and reliable heights for large parts of the glacial area. However, higher errors were observed for steep slopes and areas with shadow in the images. Hence they are excluded in this study. Overall it is observed that, SGM seems to have reliable results for low contrast areas (e.g. glaciers, snow cover), and the processing speed for elevation model generation is fast. Further, the generated elevation model along with source images and other elevation models are used to map the

glacial features, to estimate elevation changes and mass balance for a period of 14 years between 2000 and 2014. The present study concludes that

1. Accurate and High spatial resolution (1.5 m) elevation model can be generated for glaciers in the complex terrain like Indian Himalaya with a least RMSE.
2. Good gridded smoothness can be attained by using SGM algorithm.
3. Comparative analysis suggests higher accuracy in elevation and mass balance information with a good correlation
4. Mass loss of the selected glaciers are higher ( $-0.99 \pm 0.28 \text{ m.w.e.a}^{-1}$ ) during 2000 and 2011, and then decreased after 2011 ( $-0.63 \pm 0.23 \text{ m.w.e.a}^{-1}$ )

Thus, this study recommends the use of high spatial resolution elevation models on a large spatial scale over a longer period to get a detailed and clearer picture on elevation differences and mass balance of glaciers in the Himalaya, which helps the management of limited water resources for 1.4 billion people.

#### **Acknowledgements:**

Corresponding author would like to thank Chairman, Dhanekula Institute of Technology, JNTU Kakinada and Dr. Ravichandran, NCPOR for the financial and infrastructure support provided during the study. A special thanks to Dr. Tobias Bolch (University of Zurich), Dr. Ian M. Howat and Dr. Myoung-Jong Noh (Byrd polar and Climate Research Centre- Ohio State University) for the technical suggestions and support during the study. I would also like to thank USGS for providing the SRTM, LPDAAC for AST14DMO Digital Elevation Models and Soubraime, IRD France for providing the SPOT-7 data for Research purpose.

#### **References:**

1. Adina E, R., Mark W, W., & Roger G, B. (2008). Optical Remote Sensing of Glacier Characteristics: A Review with Focus on the Himalaya, *Sensors*, 8, 3355-3383. DOI: 10.3390/s8053355
2. Ahmed, N., Mahtab, A., Agrawal, R., Jayaprasad, P., Pathan, S.K., Singh, D.K. & Singh, A.K. (2007). Extraction and validation of cartosat-1 DEM. *Journal of the Indian Society of Remote Sensing*, 35(2), 121.
3. Alganci, U., Besol, B. & Sertel, E. (2018). Accuracy Assessment of Different Digital Surface Models. *ISPRS International Journal of Geo-Information*, 7(3),114.
4. Anant Kumar., Negi, H.S., Kamal Kumar., Neha Kanda., Singh K, K., Ankur Pandit, & Raaj Ramsankaran. (2018). Estimation of recent changes in thickness and mass

balance of the Patsio glacier in the Great Himalayan region using geodetic technique and ancillary data. *Geocarto International*, DOI: 10.1080/10106049.2018.1506506.

5. Azam, M.F., Wagnon, P., Vincent, C., Ramanathan, A.L., Favier, V., Mandal, A. & Pottakkal, J.G. (2014). Processes governing the mass balance of Chhota Shigri Glacier (western Himalaya, India) assessed by point-scale surface energy balance measurements. *The Cryosphere*, 8(6), 2195-2217.
6. Basnett, S., Kulkarni, A.V. & Bolch, T. (2013). The influence of debris cover and glacial lakes on the recession of glaciers in Sikkim Himalaya, India. *Journal of Glaciology*, 59(218), 1035-1046.
7. Burrough, P. A. (1986). Principles of Geographical Information Systems for Land Resources Assessment. *Oxford*: Clarendon Press.
8. Berthier, E. & Toutin, T. (2008). SPOT5-HRS digital elevation models and the monitoring of glacier elevation changes in North-West Canada and South-East Alaska. *Remote Sensing of Environment*, 112(5), 2443-2454.
9. Bolch, T., Pieczonka, T. & Benn, D.I. (2011). Multi-decadal mass loss of glaciers in the Everest area (Nepal Himalaya) derived from stereo imagery. *The Cryosphere*, 5(2), 349-358.
10. CScott W., Jeffrey S. K. & Babulal, T. (2019). UAV-Derived Himalayan Topography: Hazard Assessments and Comparison with Global DEM Products, *Drones*, 3(1), 18. doi:10.3390/drones3010018
11. Dandabathula, G. (2015). Generation of Statewide DEMs and Orthoimages—Guidelines and Methodology. *Kartografija i geoinformacije (Cartography and Geoinformation)*, 13(22), 4-19.
12. Dimri, A.P., Yasunari, T., Wiltshire, A., Kumar, P., Mathison, C., Ridley, J. & Jacob, D. (2013). Application of regional climate models to the Indian winter monsoon over the western Himalayas. *Science of The Total Environment*, 468, 36-47.
13. Droj, G. (2008). Improving the accuracy of digital terrain models. Vol. LIII. *Babes-Bolyai: Studia Universitate*.
14. Drăguț L., Eisank C., & Strasser T. (2011). Local variance for multi-scale analysis in geomorphometry. *Geomorphology*, 130, 162–172.
15. Ernst, I. & Hirschmüller, H. (2008), December. Mutual information based semi-global stereo matching on the GPU. In International Symposium on Visual Computing (228-239). Springer, Berlin, Heidelberg.
16. Fisher, P.F., & Tate, N.J. (2006). Causes and consequences of error in digital elevation models. *Progress in physical Geography*, 30(4), 467-489.
17. Goodchild, M.F. (2008). Geographic Information Science: The Grand Challenges, 39.
18. Goodchild, M.F., & Kemp, K.K. eds. (1990). NCGIA Core Curriculum in GIS.

19. Gaddam, V.K., Kulkarni, A.V. & Gupta, A.K. (2016). Estimation of glacial retreat and mass loss in Baspa basin, Western Himalaya. *Spatial Information Research*, 24(3), 257-266.
20. Gaddam, V.K., Kulkarni, A.V., Gupta, A.K. & Sharma, P. (2017a). Mass balance estimation using geodetic method for glaciers in Baspa basin, Western Himalaya. *Current Science*, 113(3), 486-492.
21. Gaddam V.K., Kulkarni, A.V., & Gupta, A.K. (2019). Assessment of the Baspa basin glaciers mass budget using different remote sensing methods and modeling techniques. *Geocarto International*, DOI: [10.1080/10106049.2018.1516247](https://doi.org/10.1080/10106049.2018.1516247)
22. Gardelle, J., Berthier, E., Arnaud, Y. & Kaab, A. (2013). Region-wide glacier mass balances over the Pamir-Karakoram-Himalaya during 1999-2011. *The Cryosphere*, 7(6), 1885-1886.
23. Giribabu, D., Kumar, P., Mathew, J., Sharma, K.P. & Murthy, Y.K. (2013). DEM generation using Cartosat-1 stereo data: issues and complexities in Himalayan terrain. *European Journal of Remote Sensing*, 46(1), 431-443.
24. Heid, T. & Kääb, A. (2012). Repeat optical satellite images reveal widespread and long term decrease in land-terminating glacier speeds. *The Cryosphere*, 6(2), 467-478.
25. Hayakawa, Y.S., Oguchi, T. & Lin, Z. (2008). Comparison of new and existing global digital elevation models: ASTER GDEM and SRTM3. *Geophysical Research Letters*, 35(17).
26. Hirschmuller, H. (2008). Stereo processing by semiglobal matching and mutual information. *IEEE Transactions on pattern analysis and machine intelligence*, 30(2), 328-341.
27. Hirschmuller, H. & Scharstein, D. (2009). Evaluation of stereo matching costs on images with radiometric differences. *IEEE transactions on pattern analysis and machine intelligence*, 31(9), 1582-1599.
28. Hirschmüller, H. (2011), September. Semi-global matching-motivation, developments and applications. *In Photogrammetric week*, 11, 173-184.
29. Heuvelink, G.B. (1998). Error propagation in environmental modelling with GIS. CRC Press.
30. Huss, M. (2013). Density assumptions for converting geodetic glacier volume change to mass change. *The Cryosphere*, 7(3), 877-887.
31. Jacobsen, K. & Passini, R. (2003). Accuracy of digital orthophotos from high resolution space imagery. In Proceedings of the Workshop High Resolution Mapping from Space.
32. Jacobsen, K. (2004). Analysis of digital elevation models based on space information. In EARSEL Symposium, Dubrovnik.



33. Jacobsen, K. (2013). Characteristics and accuracy of large area covering height models. *International Archives of the Photogrammetry, Remote Sensing and Spatial Information Sciences-ISPRS Archives* 40 (2013), 40(1W1),157-162.
34. Jacobsen, K. (2005). DEMs based on space images versus SRTM height models. In ASPRS annual convention Baltimore.
35. Kulkarni, A.V., Rathore, B.P. & Alex, S. (2004). Monitoring of glacial mass balance in the Baspa basin using accumulation area ratio method. *Current science*, 185-190.
36. Kaur, R., Kulkarni, A.V. & Chaudhary, B.S. (2010). Using RESOURCESAT-1 data for determination of snow cover and snowline altitude, Baspa Basin, India. *Annals of Glaciology*, 51(54), 9-13.
37. Kääb, A., Berthier, E., Nuth, C., Gardelle, J., & Arnaud, Y. (2012). Contrasting patterns of early twenty-first-century glacier mass change in the Himalayas. *Nature*, 488(7412), 495-498.
38. Li, Z., Zhu, Q. and Gold, C. (2004). Digital terrain modeling: principles and methodology. CRC press.
39. Lucas, B.D. and Kanade, T. (1981). An iterative image registration technique with an application to stereo vision.
40. Maurer, J. M., Rupper, S. B., & Schaefer, J. M. (2016). Quantifying ice loss in the eastern Himalayas since 1974 using declassified spy satellite imagery, *The Cryosphere*, 10, 2203-2215
41. Moore, I.D., Grayson, R. B., & Ladson, A. R. (1991). Digital terrain modelling: a review of hydrological, geomorphological, and biological application. *Hydrological Processes*, 5: 3–30
42. Mir, R.A., Jain, S.K., Jain, S.K., Thayyen, R.J. & Saraf, A.K. (2017). Assessment of recent glacier changes and its controlling factors from 1976 to 2011 in Baspa basin, western Himalaya. *Arctic, antarctic, and alpine research*, 49(4), 621-647.
43. Narendra, K. & Rao, K.N. (2006). Morphometry of the Meghadrigedda watershed, Visakhapatnam district, Andhra Pradesh using GIS and Resourcesat data. *Journal of the Indian Society of Remote Sensing*, 34(2), 101.
44. Nuth, C. & Kääb, A. (2011). Co-registration and bias corrections of satellite elevation data sets for quantifying glacier thickness change. *The Cryosphere*, 5(1), 271-290.
45. Pieczonka, T. & Bolch, T. (2015). Region-wide glacier mass budgets and area changes for the Central Tien Shan between~ 1975 and 1999 using Hexagon KH-9 imagery. *Global and Planetary Change*, 128, 1-13.
46. Pratap, B., Dobhal, D.P., Rakesh, B., Mehta, M. & tiwari, V.C. (2016). Four decades of glacier mass balance observations in the Indian Himalaya. *Regional Environmental Change*, 16(3), 643-658.

47. Prasad V., Kulkarni, A.V., Praeep, S., Pratibha, Tawde, S.A., Shrisat, T., Arya., Andreworr & Daniel, B. (2019). Large losses in glacier area and water availability by the end of twenty first century under high emission scenario, satluj basin, Himalaya. *Current Science*, 116(10), 1721-1730.
48. Rajesh, K., Singh, S., Kumar, R., Singh, A., Bhardwaj, A., LydiaSam., Randhawa, S.S. & Gupta. A. (2018). Development of a Glacio-hydrological Moel for Discharge and Mass balance Reconstruction. *Water Resources Management*, 30(10), 3475-3492.
49. Rosenholm, D.A.N. & Torlegard, K. (1988). Three-dimensional absolute orientation of stereo models using digital elevation models. *Photogrammetric engineering and remote sensing*, 54(10), 1385-1389.
50. RGI Consortium. (2017). Randolph Glacier Inventory – A Dataset of Global Glacier Outlines: Version 6.0: Technical Report, Global Land Ice Measurements from Space, Colorado, USA. Digital Media. DOI: <https://doi.org/10.7265/N5-RGI-60>
51. Rignot, E., Echelmeyer, K., & Krabill, W. (2001). Penetration depth of interferometric synthetic aperture radar signals in snow and ice. *Geophysical Research Letters*, 28(18), 3501- 3504.
52. Sangewar & S.P. Shukla, GSI (2009). Inventory of the Himalayan Glaciers : A Contribution to the International Hydrological Programme [Special Publication No. 34, *Geological Survey of India*]:
53. San, B.T. & Suzen, M.L. (2005). Digital elevation model (DEM) generation and accuracy assessment from ASTER stereo data. *International Journal of Remote Sensing*, 26(22), 5013-5027.
54. Shukla, A., Arora, M.K. & Gupta, R.P. (2010). Synergistic approach for mapping debris-covered glaciers using optical–thermal remote sensing data with inputs from geomorphometric parameters. *Remote Sensing of Environment*, 114(7), 1378-1387.
55. Toutin, T. (2008). ASTER DEMs for geomatic and geoscientific applications: a review. *International Journal of Remote Sensing*, 29(7), 1855-1875.
56. Wise, S. (2011). Cross-validation as a means of investigating DEM interpolation error. *Computers & Geosciences*, 37(8), 978-991.
57. Wendt, A., Mayer, C., Lambrecht, A., Völksen, C., & Floricioiu, D. (2017). Elevation Changes and Ice Flow Velocities of Fedchenko Glacier and its Tributaries in the Pamir Mountains.
58. Watson, C.S., Kargel, J.S. & Tiruwa, B. (2019). UAV-Derived Himalayan Topography: Hazard Assessments and Comparison with Global DEM Products. *Drones*, 3(1), 18.

## **Figures Subtitles:**

Figure 1a. Geographical location of glaciers in the Himachal Pradesh, Indian Himalaya.

Figure 1b. Glaciers chosen for the elevation model generation. The glaciers map shows the glaciers area, maximum length, snout altitudes and field control points

Figure 2. Flowchart for estimation of elevation models using SPOT datasets

Figure 3a. The las image files of Jorya garang glacier

Figure 3b. The las image files of Shaune garang glacier

Figure 4. Areal extents and elevation information of glaciers mapped using SPOT-7 imagery

Figure 5. Quantitative assessment for elevation points from SPOT-7 and from field surveyed GCP points.

Figure 6a. Discrepancies existing in glaciers area of SG, NG, JG from various inventories

Figure 6b. Discrepancies existing in glaciers area of GG and GK from various inventories

Figure 7. Estimates of supraglacial debris cover on all the five glaciers, and shown with pink color boundary.

Figure 8. Lake extents on supra-glacial and peri-glacial zones of selected glaciers

Figure 9. Modeling registration error, before and after coregistration

Figure 10a. Elevation changes observed between 2000 and 2011, using SRTM and ASTER dataset

Figure 10b. Elevation changes observed between 2011 and 2014, using ASTER and SPOT dataset

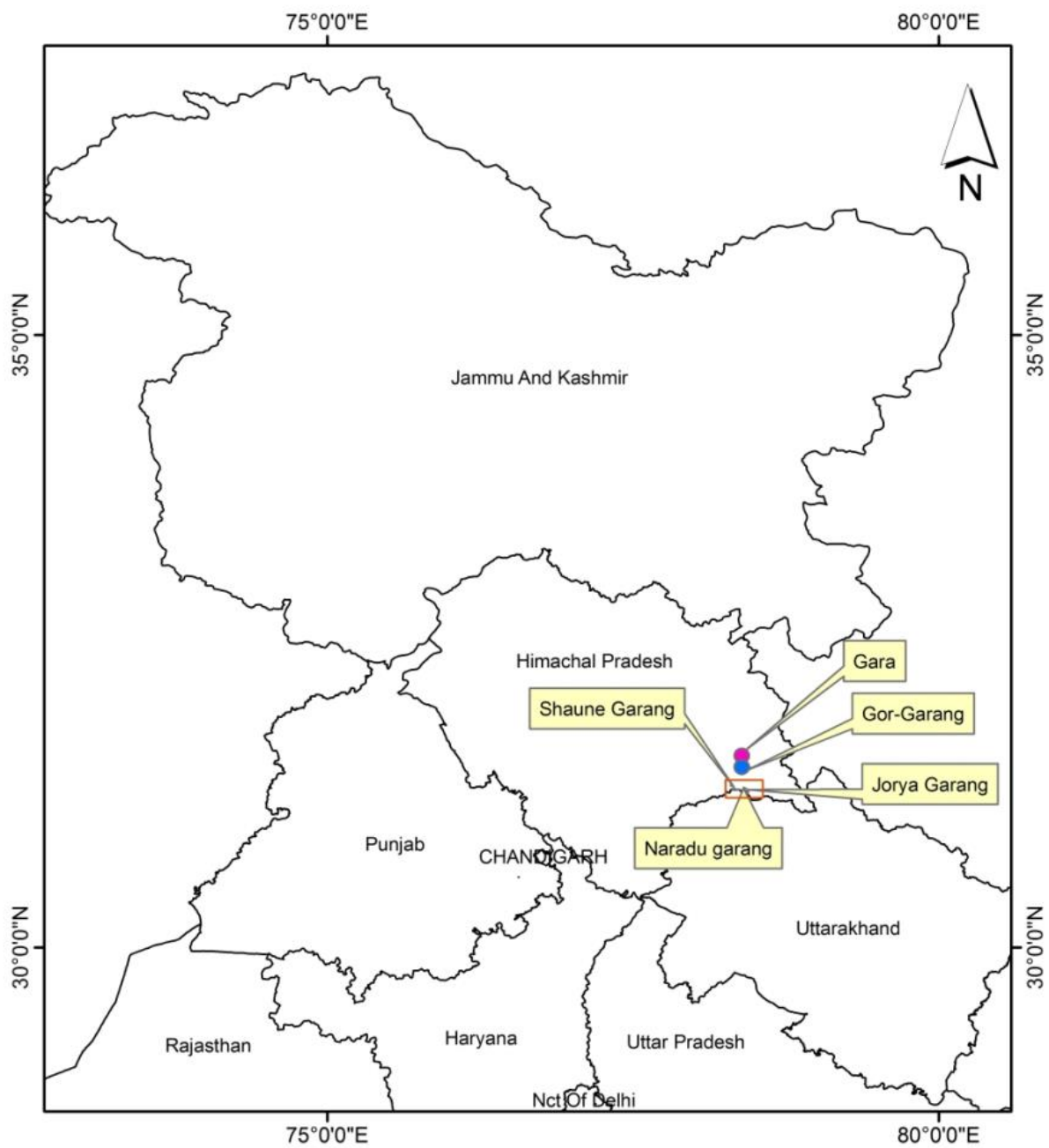


Figure 1

359x375mm (300 x 300 DPI)

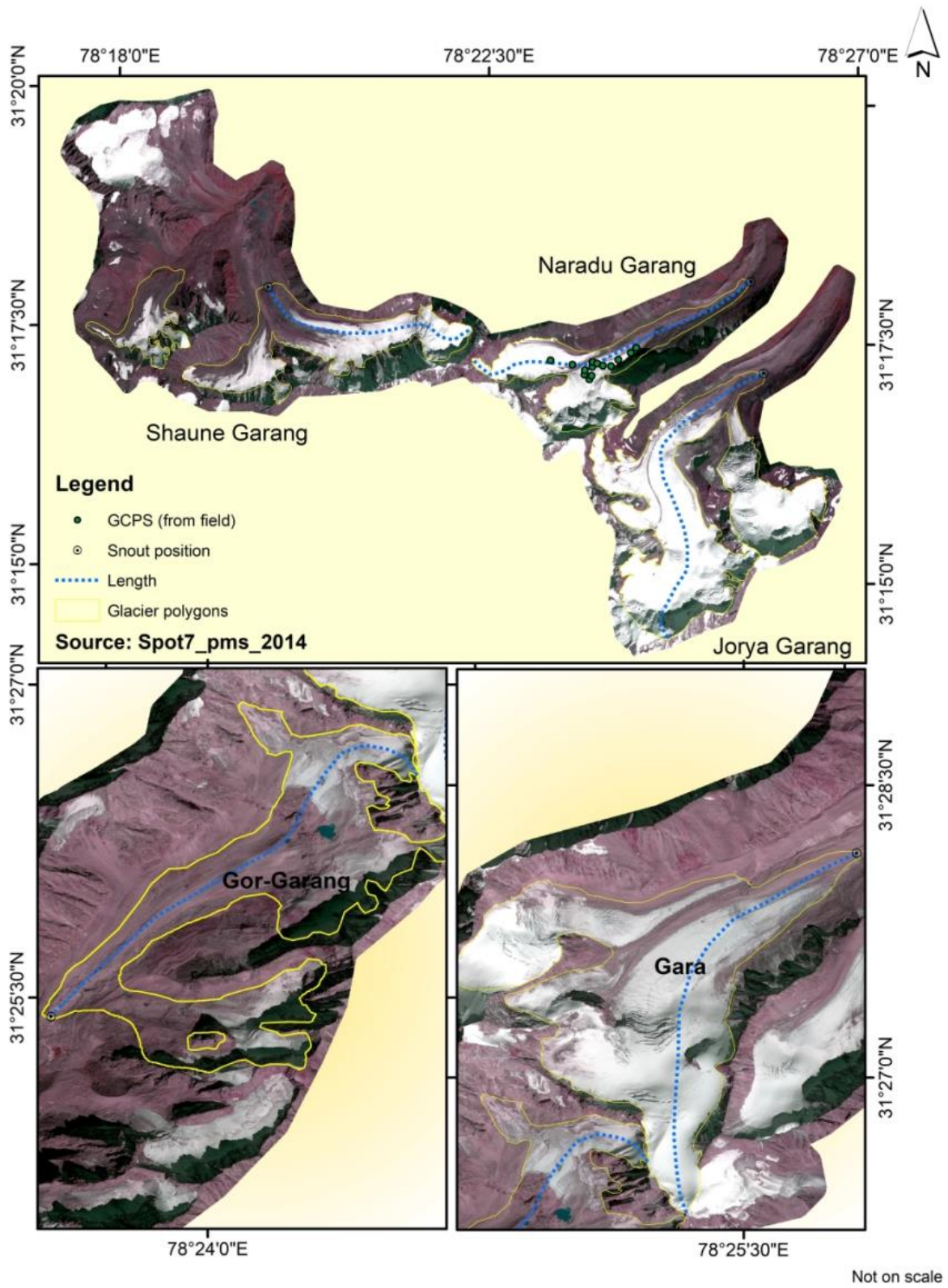


Figure 1b

431x558mm (300 x 300 DPI)

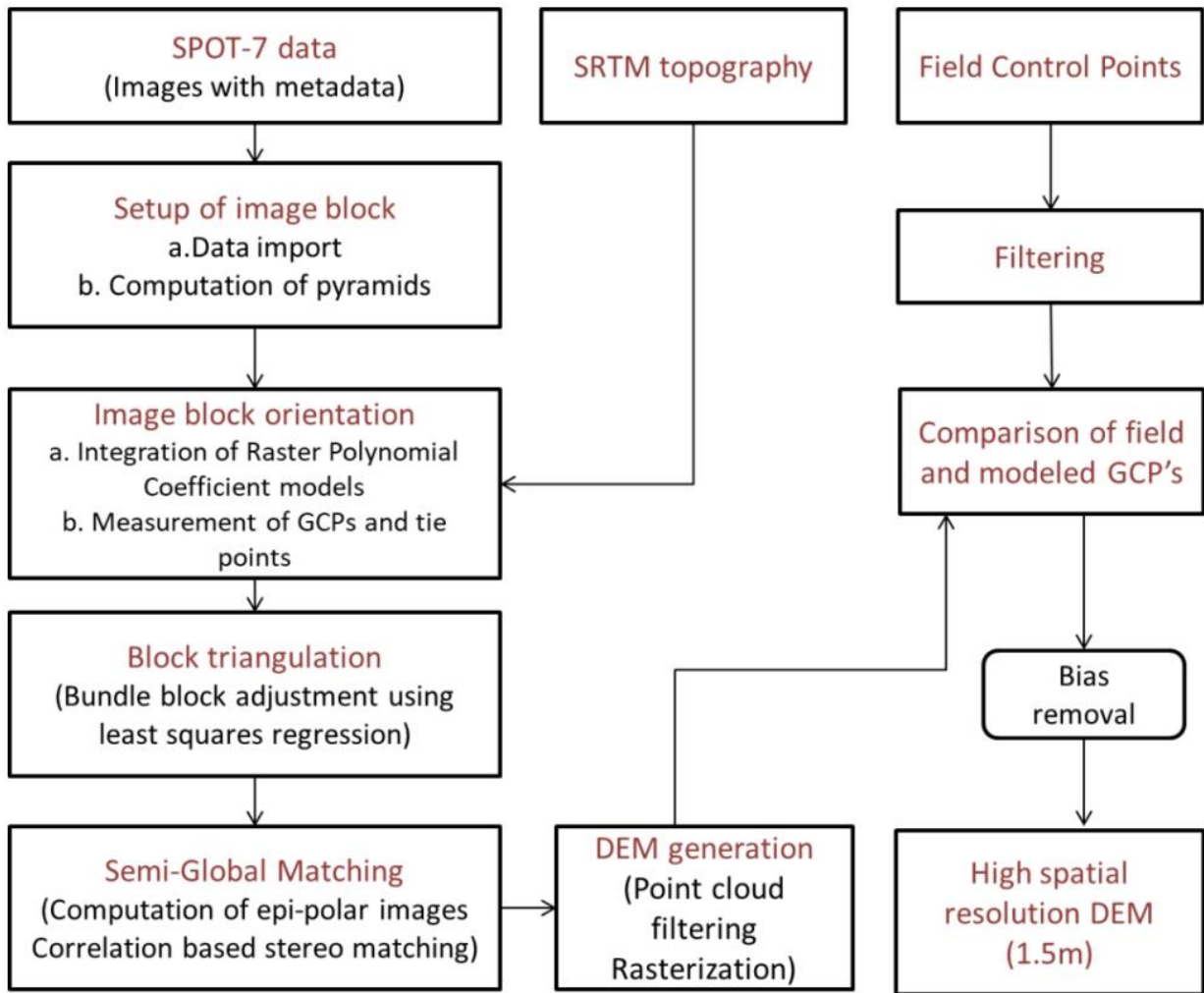


Figure 2

101x84mm (300 x 300 DPI)

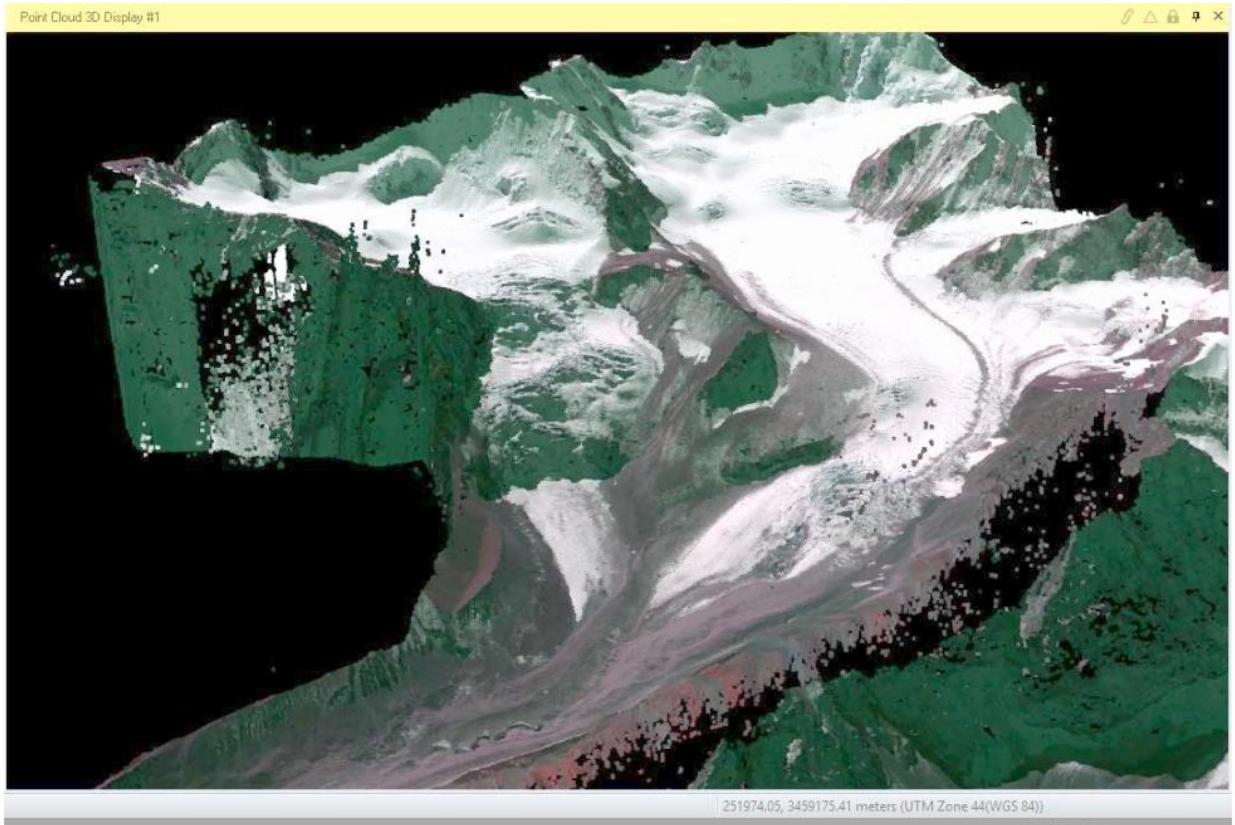


Figure 3a

91x61mm (300 x 300 DPI)

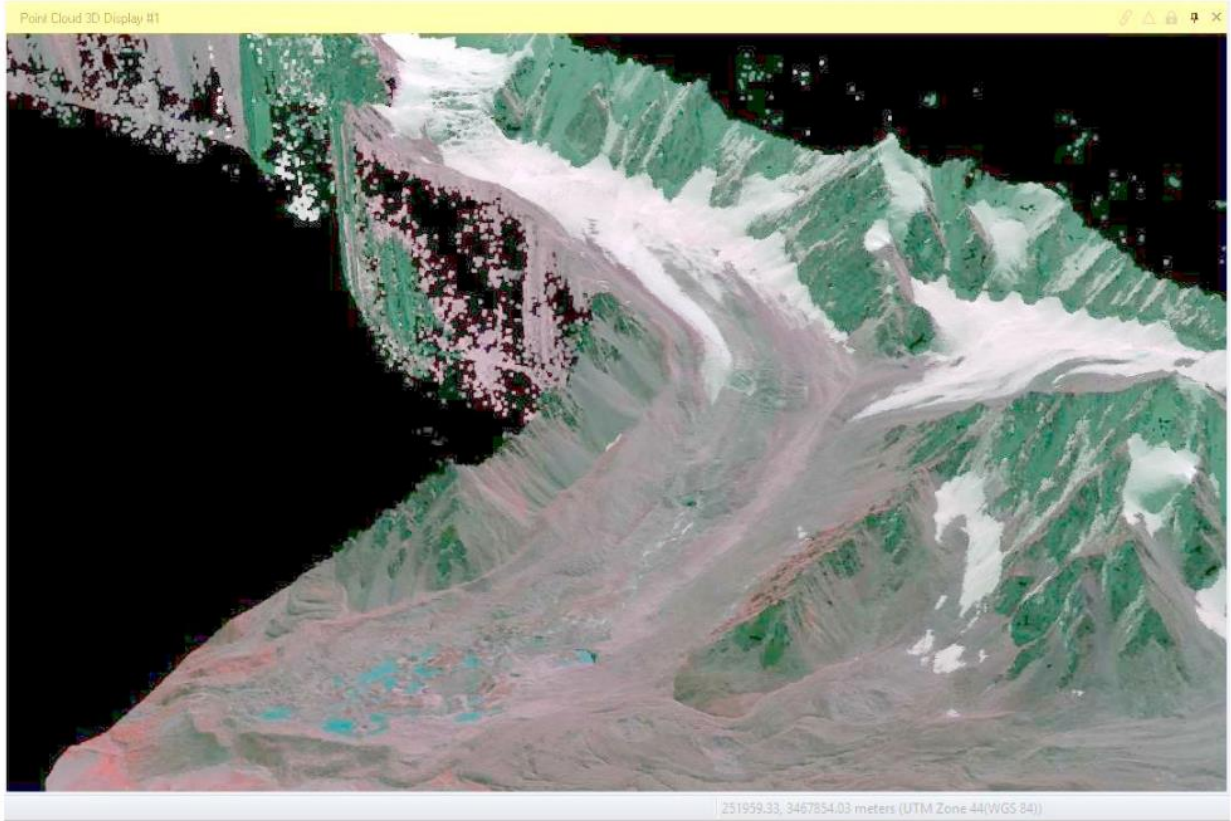


Figure 3b

91x61mm (300 x 300 DPI)



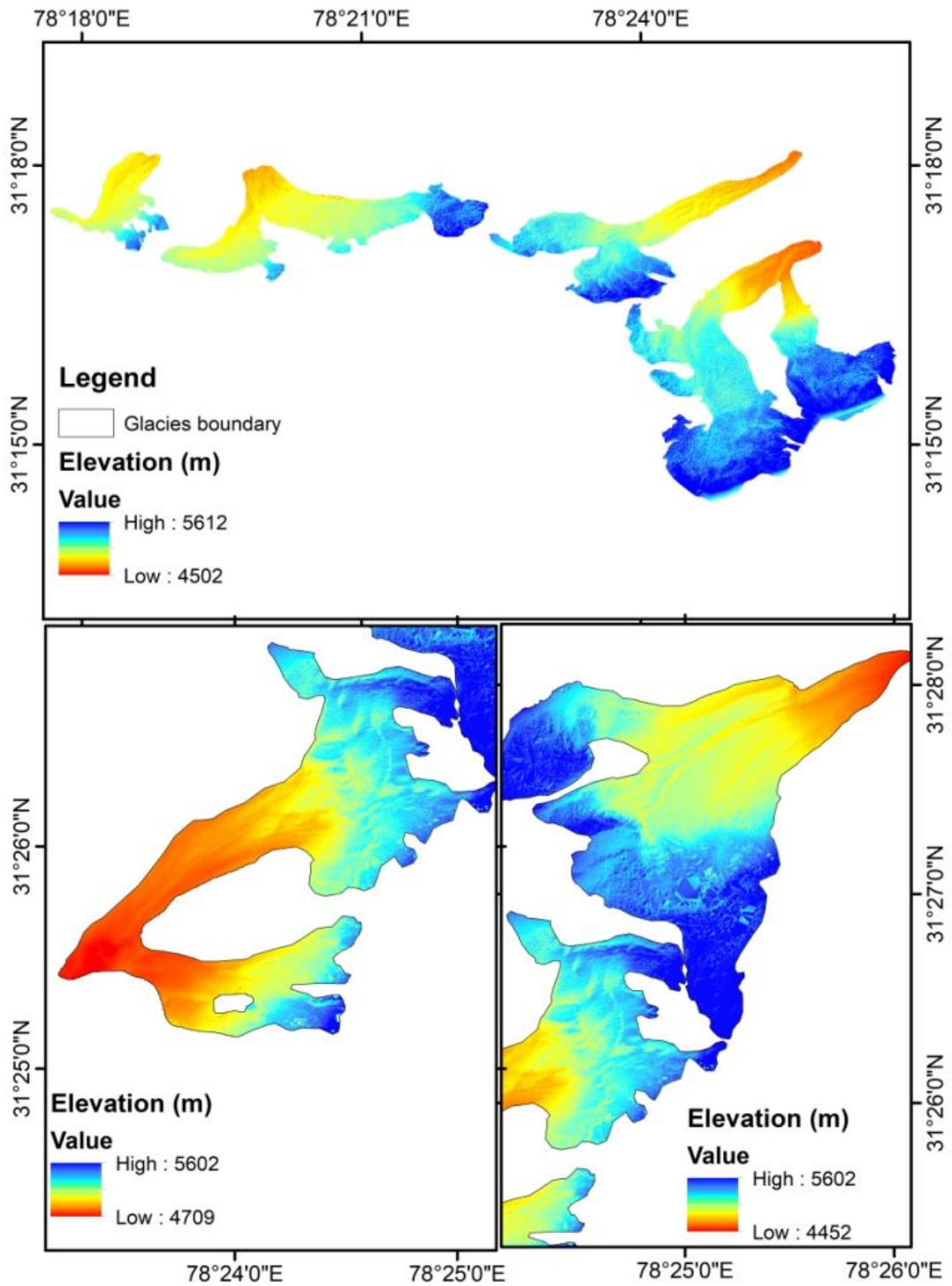


Figure 4

431x558mm (300 x 300 DPI)

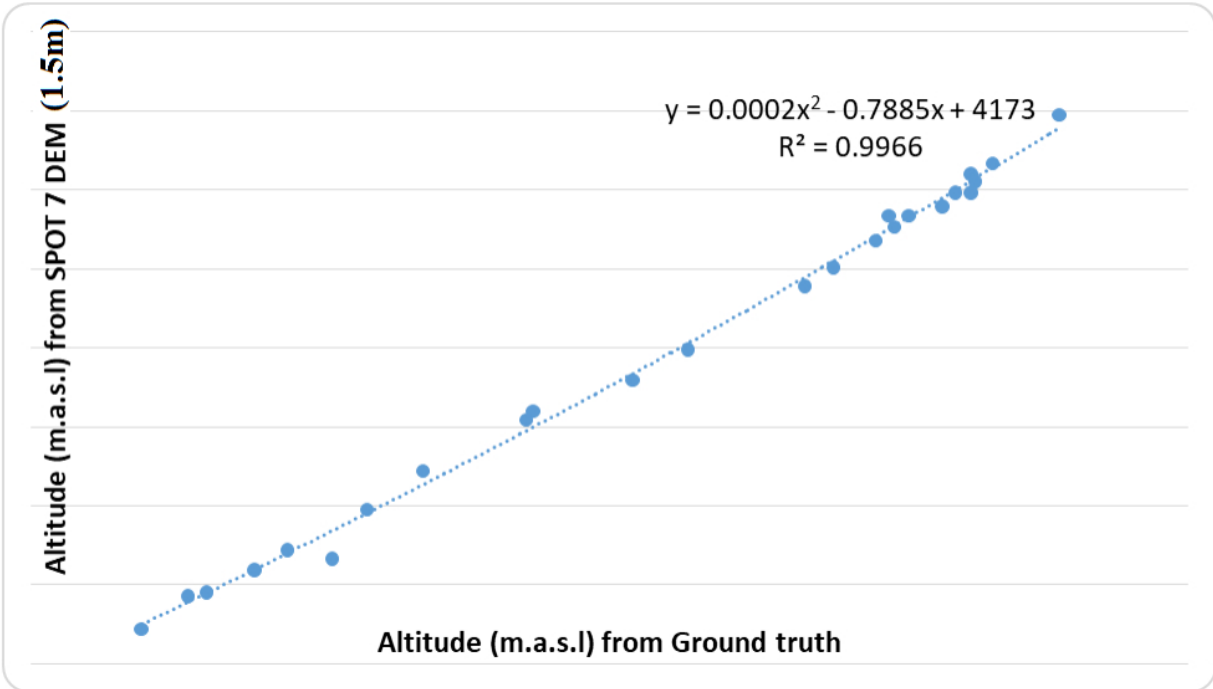


Figure 5

82x46mm (300 x 300 DPI)

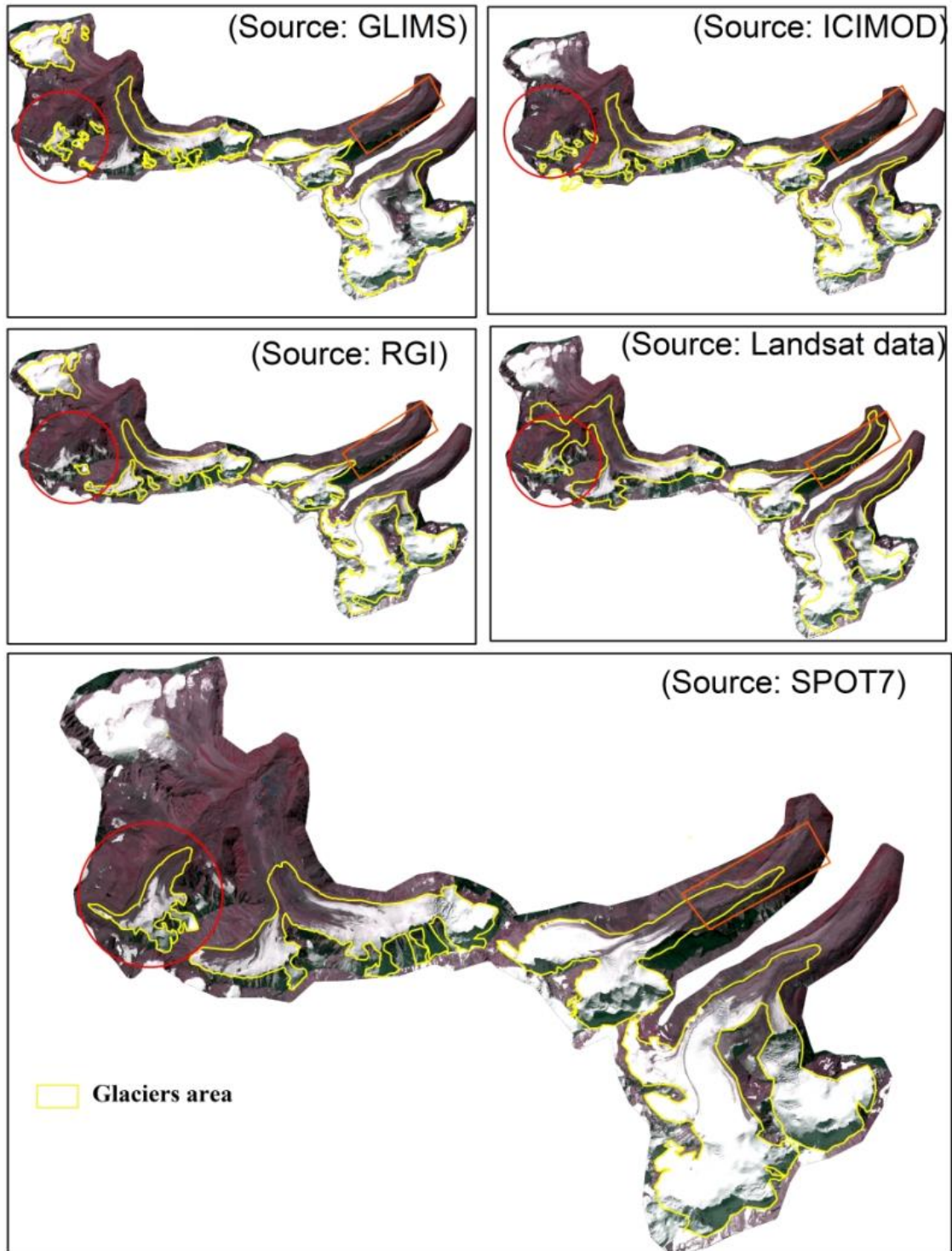


Figure 6a

359x465mm (300 x 300 DPI)

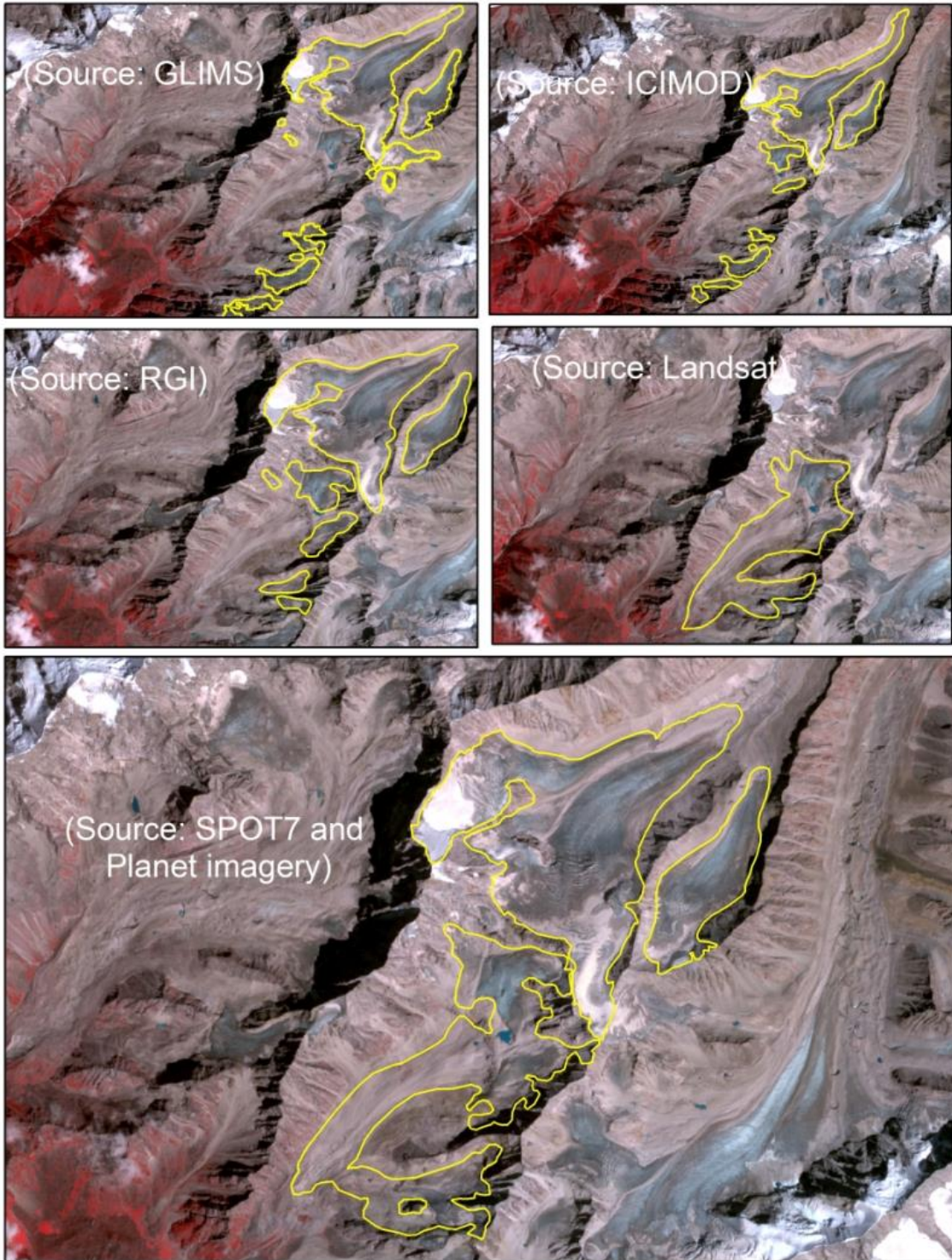


Figure 6b

287x372mm (300 x 300 DPI)

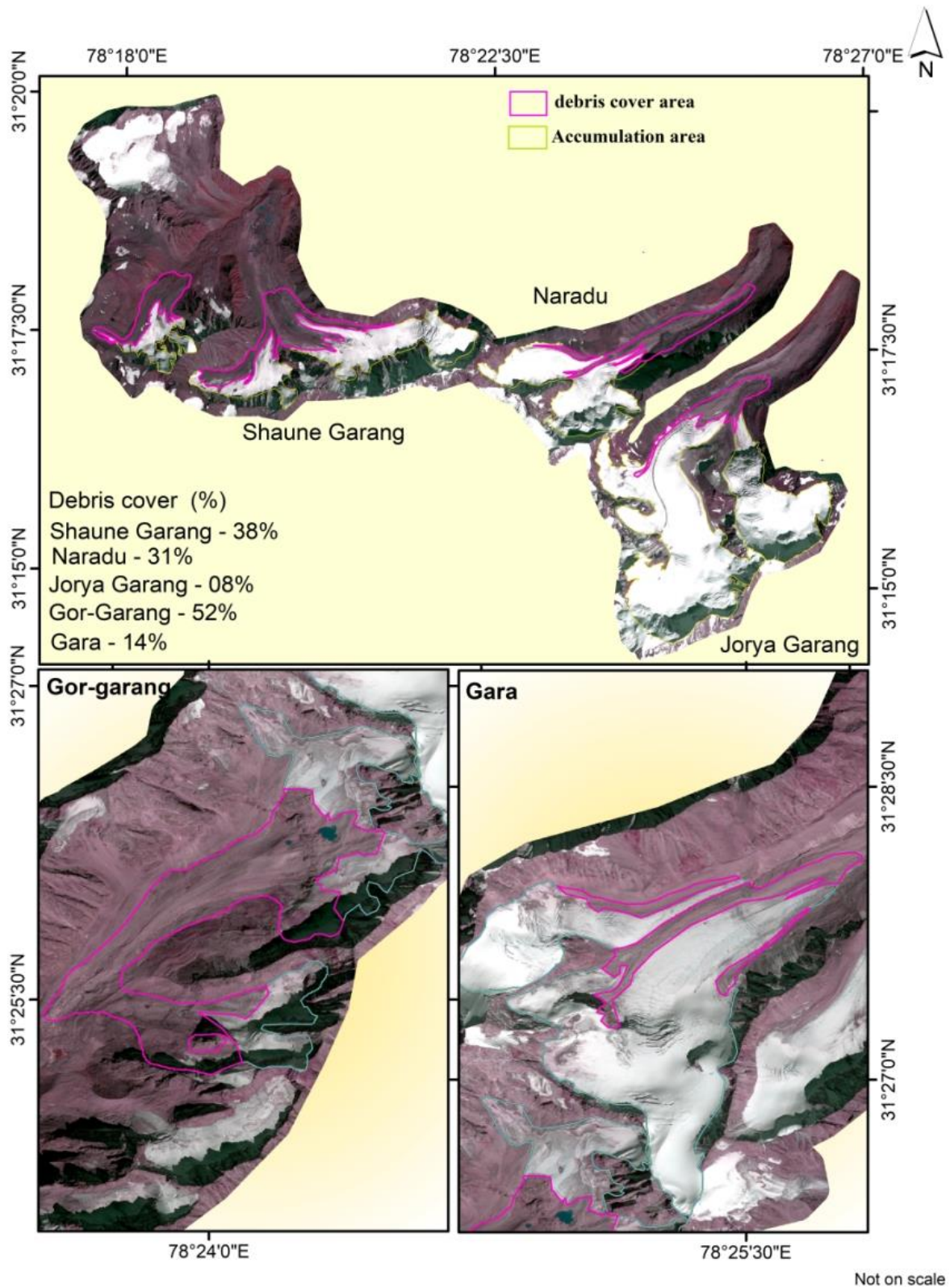


Figure 7

431x558mm (300 x 300 DPI)

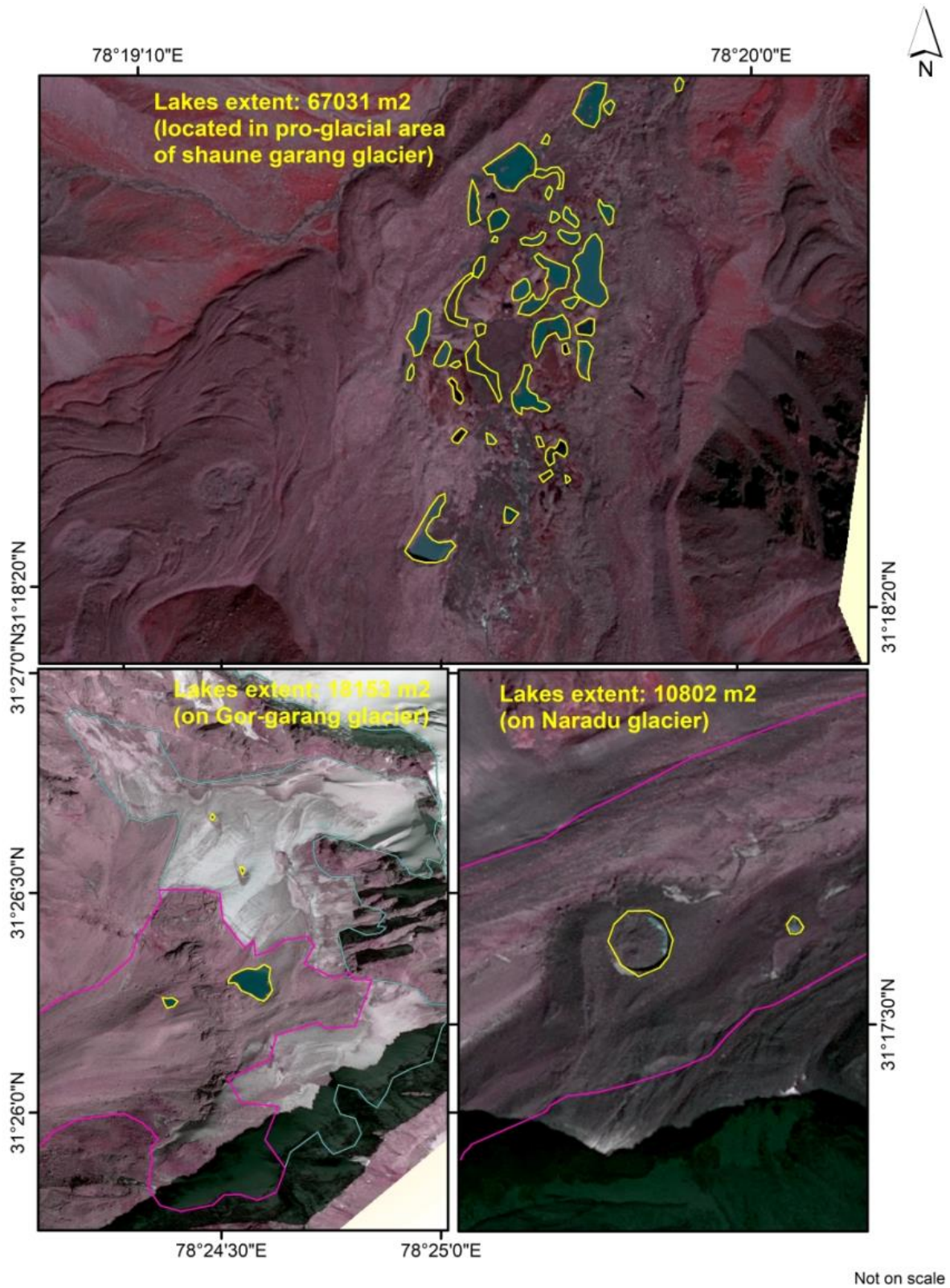


Figure 8

431x558mm (300 x 300 DPI)

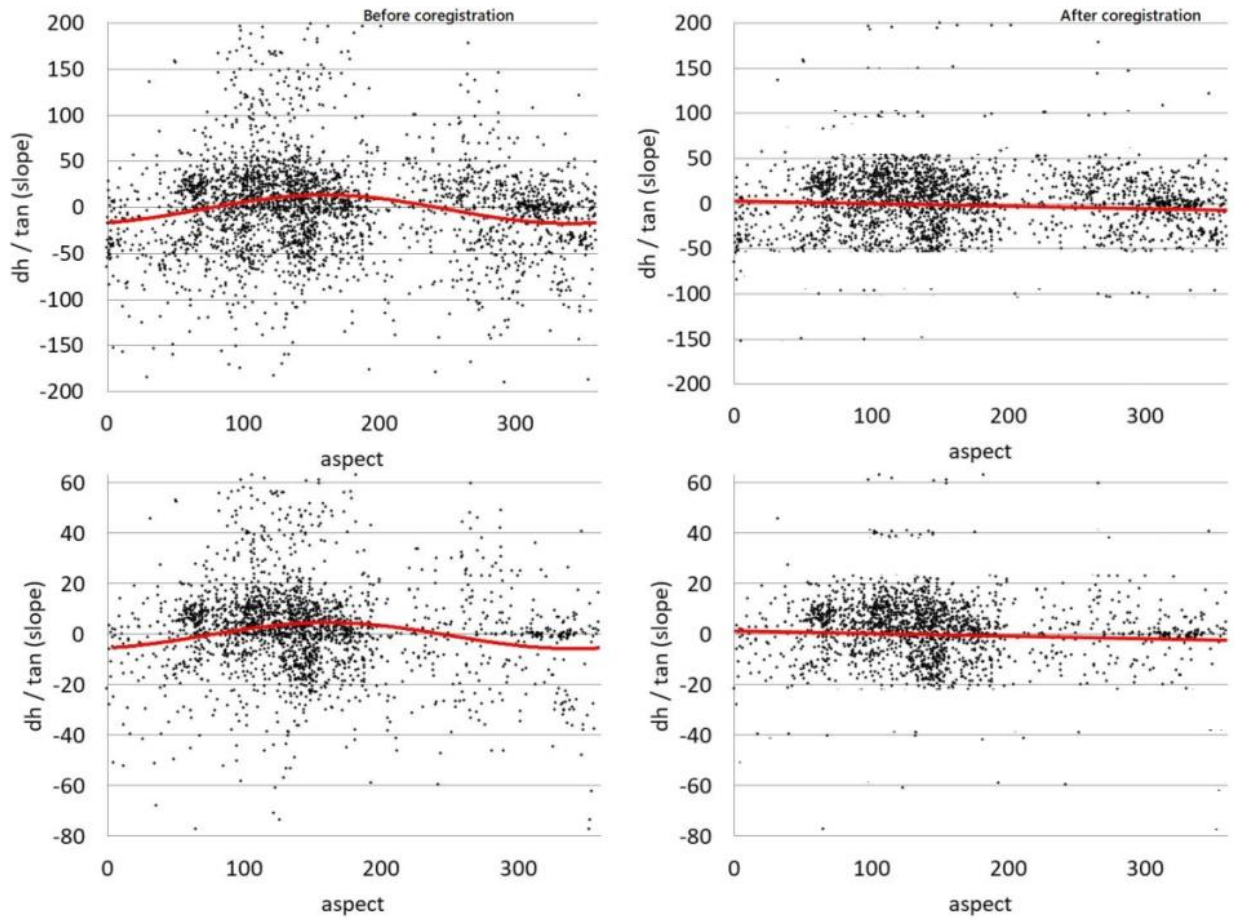


Figure 9

127x92mm (300 x 300 DPI)

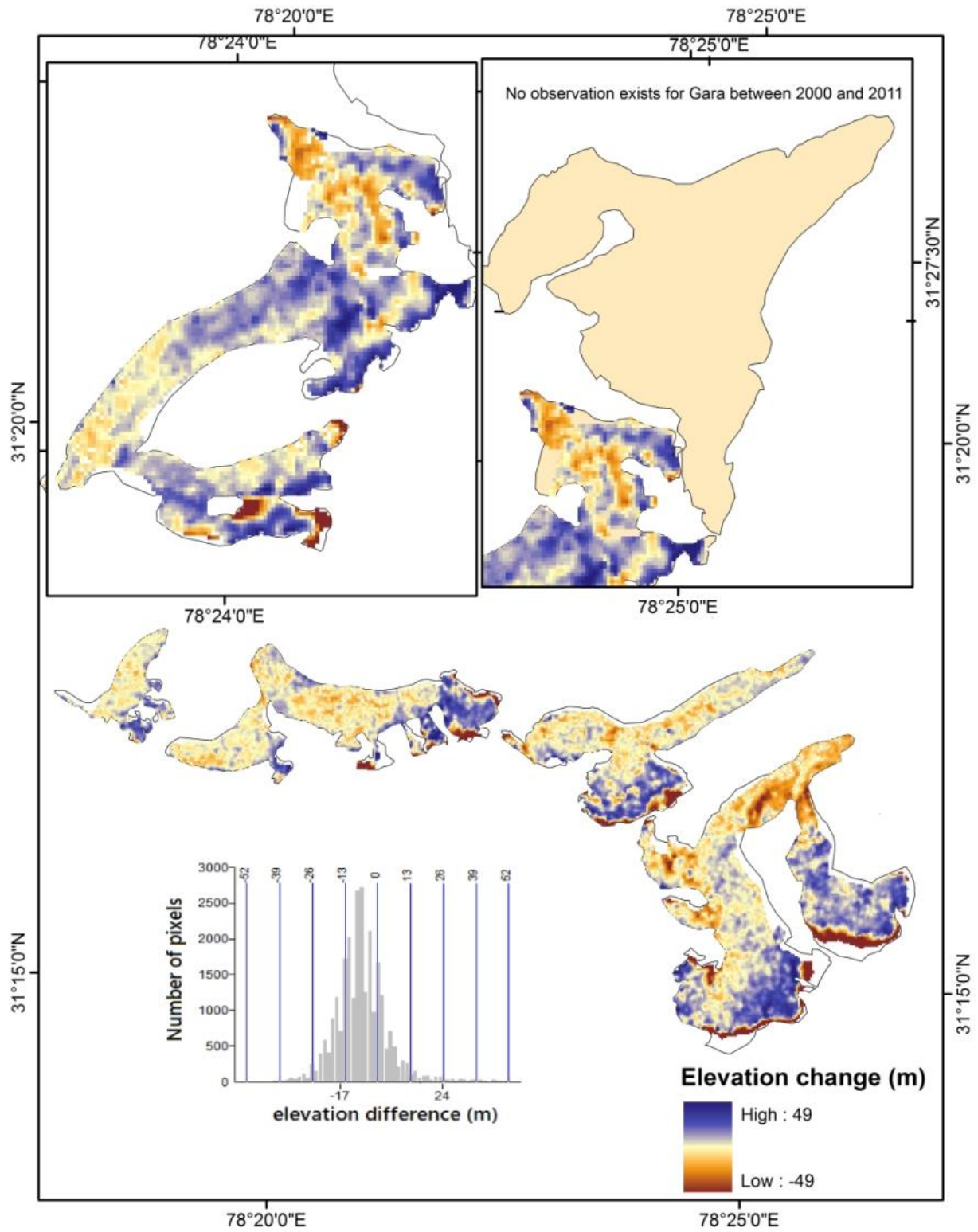


Figure 10a

359x465mm (300 x 300 DPI)



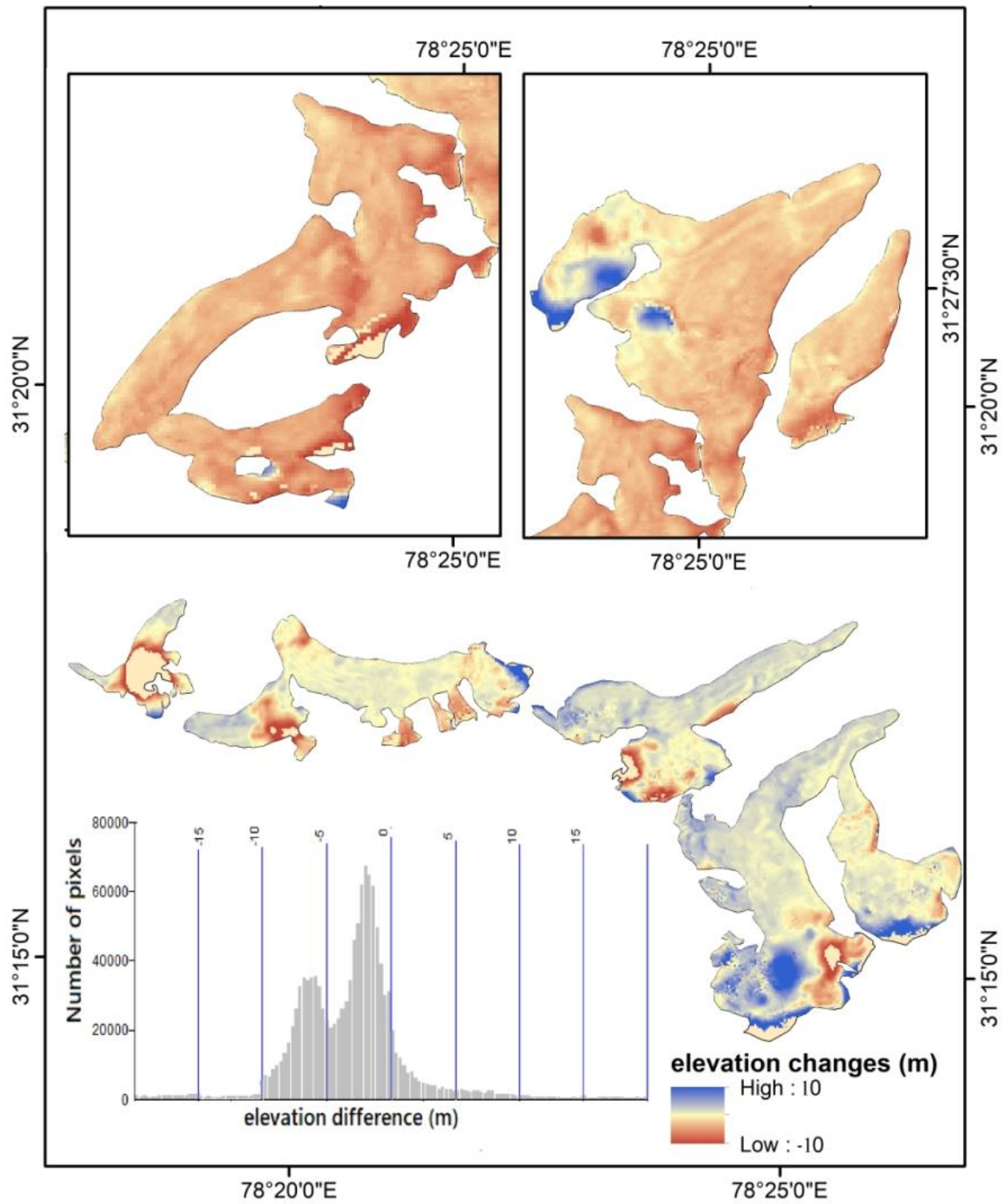


Figure 10b

330x377mm (300 x 300 DPI)

Table 1. Areal extents mapped in the present study and from the literature. Snout altitude during the maximum glaciation time is also given in the table.

S.No	Glacier Name	Reported Area (km <sup>2</sup> )	Area mapped using SPOT-7 data (km <sup>2</sup> )	Present altitude of Snout $\pm$ error (m.a.s.l.)	Reported altitude (m.a.s.l.)	Snout at maximum glaciation	References
1	Gor garang	3.8 $\pm$ 0.29	3.40 $\pm$ 0.28	4703 $\pm$ 6	4757 (field)	4561	Deota et al 2011
2	Shaune garang	6.03 $\pm$ 0.44	6.01 $\pm$ 0.50	4505 $\pm$ 6	4512 (field)	4172	Sangewar and Shukla, 2009
3	Jorya garang	9.7 $\pm$ 0.53	10.37 $\pm$ 0.86	4447 $\pm$ 6	4349 (field)	4062	Sangewar and Shukla, 2009
4	Naradu garang	3.79 $\pm$ 0.27	4.05 $\pm$ 0.34	4513 $\pm$ 6	4508 $\pm$ 8 (field in 2014 survey) 4518 $\pm$ 21 (mapping) 4484 (field in 2005 survey)	4281	Gaddam et al 2016 Deota et al 2011
5	Gara Kund	4.28 $\pm$ 0.22	4.32 $\pm$ 0.36	4712 $\pm$ 6	4710 (field)	-n/a-	Raina et al 2000

Table 2. Mass loss observations between 2000 and 2011, with respect to 2011 and 2014, and from literature

Glacier name	mid-altitude	2000-2011		2011-2014		From literature	
		Geodetic	error	mass loss per year	error per year	mass loss per year (periods of observation)	References
JG	5050	-1.19	0.23	-0.40	0.24		
NG	5100	-0.83	0.26	-0.71	0.36	-0.40 (2000-2003)	Pratap et al 2016, Prasad et al 2019 Kumar et al 2018
SG	5050	<b>-0.99</b>	<b>0.35</b>	-0.59	0.41	-0.42 (1982-1992) -0.59 (1985-1991) <b>-0.89 (2001-2008)</b>	Pratap et al 2016 Prasad et al 2019 Kumar et al 2018
GG	5200	-0.98	0.26	-0.80	0.35	-0.38 (1977-1986)	Pratap et al 2016
GK	5155	-	-	-0.54	0.17		
Average	5111	<b>-0.99</b>	<b>0.27</b>	<b>-0.61</b>	<b>0.31</b>		